Nonlinear waves in networks: model reduction for sine-Gordon

Jean-Guy Caputo, Denys Dutykh

Jean-Guy Caputo
INSA de Rouen, France

Denys Dutykh
CNRS–LAMA, University of Savoie, France

Nonlinear waves in networks: model reduction for sine-Gordon

Last modified: November 3, 2016

Nonlinear waves in networks: model reduction for sine-Gordon

Jean-Guy Caputo and Denys Dutykh

Abstract. To study how nonlinear waves propagate across Y- and T-type junctions, we consider the 2D sine-Gordon equation as a model and examine the crossing of kinks and breathers. Comparing energies for different geometries reveals that, for small widths, the angle of the fork plays no role. Motivated by this, we introduce a 1D effective model whose solutions agree well with the 2D simulations for kink and breather solutions. These exhibit two different behaviors: a kink crosses if it has sufficient energy; conversely a breather crosses when $v > 1 - \omega$, where v and ω are respectively its velocity and frequency. This methodology can be generalized to more complex nonlinear wave models.

Key words and phrases: sine-Gordon equation; kink; breather; networks; Josephson junction

MSC: [2010] 35R02 (primary), 34B45 (secondary)
PACS: [2010] 05.45.Yv (primary), 74.81.Fa (secondary)

Key words and phrases. sine-Gordon equation; kink; breather; networks; Josephson junction.

Contents

1. Introduction

The propagation of nonlinear waves in networks is a very common problem. Examples are the nerve impulse traveling in arrays of neurons [14], the motion of the pulse wave in the arterial circulatory system [13] or the propagation of waves in the electrical power grid [1]. In general the problem is difficult to tackle because both the equation of motion and the geometry are complex. A first direction is to consider a simpler geometry like a Y-junction, see Fig. 1. Another simplification is to study what happens for a linear wave equation. In this context, a number of researchers have examined so-called quantum graphs where the Schrödinger equation is solved on a network. See [7] for a review. For these linear systems, the scattering formalism can be employed and this gives the reflection and transmission coefficients for a harmonic wave. This is detailed specifically for a Y-junction and for the Klein–Gordon linear wave equation in [3].

In many cases however, the nonlinearity cannot be neglected. For fluid systems, note the works by Bona and Cascaval [4] and Mugnolo and Rault [11] who used the Benjamin–Bona–Mahoney (BBM) shallow water equation to describe a fluid network. The authors used the fact that the BBM equation is unidirectional, hence, most of the energy is propagated downstream. For the Boussinesq equation in a junction, Nachbin and Da Silva Simoes [12] used a conformal map technique. However, all these studies do not provide a simple understanding of the behavior of the waves, in particular one cannot see easily how energy travels across the network.

To address these issues, a first step is to consider a simpler model. For instance, before tackling the propagation of shallow water waves in a river basin, for which there are two variables, the water elevation and the potential flow, it is useful to consider a simpler nonlinear hyperbolic equation. The sine-Gordon equation is precisely a simple nonlinear hyperbolic equation that admits localized solutions. It is also a Hamiltonian system in any dimension, integrable in 1D so that one can compare the numerical solutions with their exact counterpart as they propagate in a 1D channel. Finally, the sine-Gordon equation is an excellent model of an extended Josephson junction between two superconductors [2]. Here, to simplify the issue and to keep the Hamiltonian framework, we exclude external actions on the network, like a current or a magnetic field, that are commonly used in Josephson junction arrays.

Consider the 2D sine-Gordon equation defined in a Y-junction such as shown in Fig. 1. A first work on the problem is by Gulevich and Kusmartsev [8] who examined numerically how kinks propagate in such a system, in the context of Josephson junctions. They showed that the kink needs a sufficient velocity to cross the branch. Here we follow up on this and define a 2D symmetric junction parameterized by the angle θ between the branches and by the widths $w_{1,2}$ of the branches. This setup can describe a Y-junction up to a T-junction ($\theta = 180°$). We solve the 2D problem using the `FreeFem++` finite element library [10]. It is important that the energy is conserved by the code; for this we found a suitable time discretisation. The study of the propagation of a kink in the junction yielded the

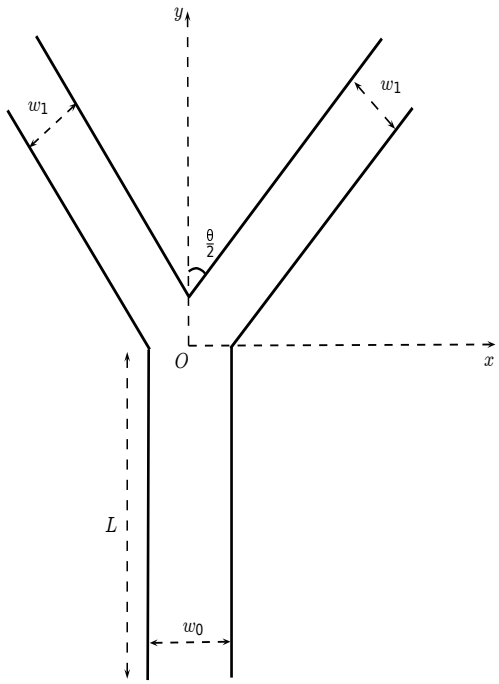

Figure 1. *Sketch of the computational domain* Ω.

immediate result, that for small widths, there is no dependence of the velocity on the angle of the fork for the full 2D simulation. We therefore introduce a 1D effective partial differential equation to capture the essential features of the 2D propagation. This model incorporates the junction, using the ideas of graph Laplacian [5]; its solutions agree well with the 2D solutions. For the kink propagation in a junction we confirm the existence of a critical velocity given approximately by the simple energy conservation argument. Below this velocity, the kink gets reflected by the fork. Above it, it passes through the junction and splits into two kinks that propagate in the two different branches. For breathers there are two parameters, ω the frequency and v the velocity. For a given velocity v, junction crossing is only possible above the frequency $\omega \approx 1 - v$ indicating a nonlinear resonance. After the breather passes through the junction it gives rise to new breathers in the branches. We characterize these using their energy density and estimate their velocity and frequency. We always observe an up-shift of the frequency and a slight down-shift of the velocity.

The article is organized as follows. In Section 2 we derive the 1D effective model from the 2D sine-Gordon equation defined in the fork. In Section 3 we recall the energies for the kink and the breather and show how they can be used to estimate a critical velocity. Section 4 introduces energy conserving discretisations for the finite element 2D problem and the 1D effective equation. Their solutions are compared in section V for both kink and breather initial conditions. Conclusions are presented in Section 5.

2. The 1D effective sine-Gordon model

We consider the 2D sine-Gordon equation

$$\phi_{tt} - \Delta\phi + \sin\phi = 0, \tag{2.1}$$

on a bounded domain $\Omega \subset \mathbb{R}^2$ with Neuman boundary conditions:

$$\nabla\phi \cdot \mathbf{n} = 0,$$

where $\mathbf{n}$ is an exterior normal. The t subscript indicates the time derivative and Δ is the usual Laplacian in spatial coordinates. This equation conserves the energy

$$\mathcal{E} = \int_\Omega \left[\frac{1}{2}\phi_t^2 + \frac{1}{2}|\nabla\phi|^2 + (1-\cos\phi)\right] \mathrm{d}x\,\mathrm{d}y. \tag{2.2}$$

This can be checked easily by multiplying (2.1) by ϕ_t, integrating over the domain and using the Stokes formula for the spatial operator.

Since the boundary conditions of the 2D problem are homogeneous Neuman it is natural to assume that the solution is uniform in the transverse direction. In other words we keep only the first transverse Fourier mode. Then equation (2.1) reduces in each branch to a 1D sine-Gordon equation,

$$\phi^i_{tt} - \phi^i_{xx} + \sin\phi^i = 0,\ \ i = 1, 2, 3\ , \tag{2.3}$$

where the label i corresponds to the three branches as shown in Fig. 2. These equations are coupled at the apex by two conditions; one is the continuity of ϕ^i

$$\phi^1(x = l) = \phi^2(x = 0) = \phi^3(x = 0)\ , \tag{2.4}$$

and the other is the flux conservation or the Kirchoff law

$$-\,w_1\phi^1_x + w_2\phi^2_x + w_3\phi^3_x = 0, \tag{2.5}$$

where ϕ^i_x is the normal velocity in branch i. Let us now briefly justify this flux relation. For that, consider the fork domain F obtained by taking the normals at the different branches as close as possible to the fork as shown in Fig. 3. Integrating the two-dimensional equation (2.1) on F yields

$$\int_F (\phi_{tt} + \sin\phi)\,\mathrm{d}x\mathrm{d}y - \int_{\partial F} \nabla\phi \cdot \mathbf{n}\,\mathrm{d}s = 0, \tag{2.6}$$

where $\mathbf{n}$ is the normal to the edge of the domain ∂F. The second term is equal to the left hand side of (2.5). The first one is of order w^2 where w is the typical width of the branches. In the limit of small w, such that $w_i \to 0$ with w_2/w_1 and w_2/w_1 constant, the first term vanishes while the second one remains, yielding (2.5).

The numerical scheme used to solve this 1D effective model is described below (see Section 4); it is a finite difference approximation. The junction corresponds to the four nodes highlighted on Fig. 2; these are labeled as 1, 2, 3 for the three branches and are connected to the central node 4. The outer nodes are the last nodes updated by the PDE solver; let us name the value of the solution there ϕ_1, ϕ_2, ϕ_3 for each branch. The value at

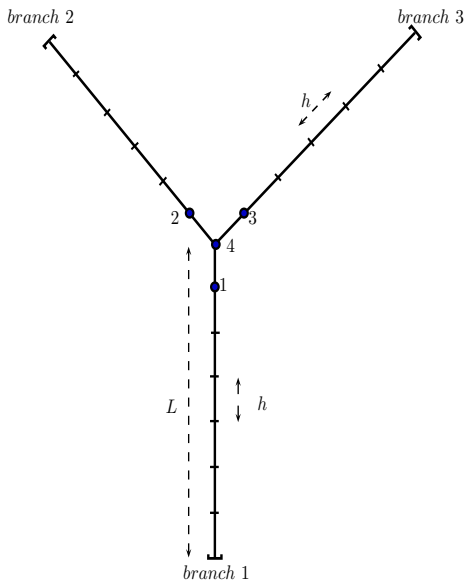

Figure 2. *Sketch of the tree geometry for the 1D effective model.*

the central node ϕ_4 can be computed from the interface conditions (2.4) and (2.5). Using a forward finite difference approximation for ϕ_x^i we get from (2.5)

$$-w_1(\phi_4 - \phi_1) + w_2(\phi_2 - \phi_4) + w_3(\phi_3 - \phi_4) = 0,$$

where we have assumed the same space step on the three branches and used the notation $\phi_i \equiv \phi(x_i)$. We have also omitted the j index corresponding to the different branches. We then obtain

$$\phi_4 = \frac{w_1\phi_1 + w_2\phi_2 + w_3\phi_3}{w_1 + w_2 + w_3}. \tag{2.7}$$

3. Theoretical considerations

In 1D the sine-Gordon equation is integrable, see for example [14]. It has two families of localized exact solutions, the kink

$$\phi(x,t) = 4\arctan\left[\exp(\gamma(x - vt))\right], \tag{3.1}$$

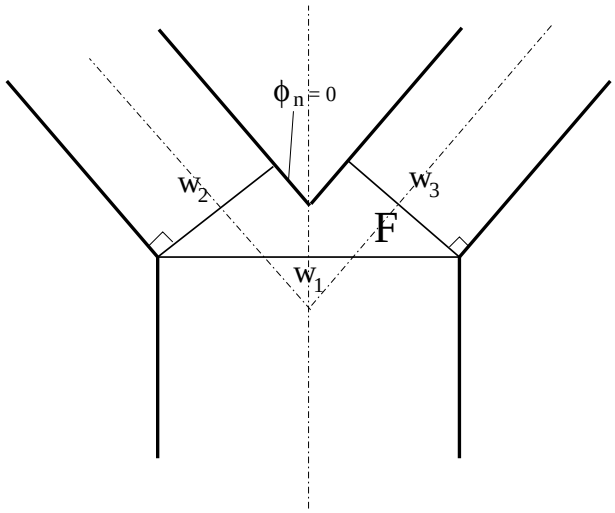

Figure 3. *The fork region F.*

and the breather [6]

$$\phi(x,t) = 4\arctan\left[\frac{\sqrt{1-\omega^2}\cos(\omega\gamma(t-vx))}{\omega\cosh(\sqrt{1-\omega^2}\gamma(x-vt))}\right], \tag{3.2}$$

where the Lorentz factor γ is given by

$$\gamma = \frac{1}{\sqrt{1-v^2}}. \tag{3.3}$$

Let us first consider the kink, its energy is

$$\mathcal{E}_k = 8\gamma. \tag{3.4}$$

The energy of the breather depends also on the frequency, it is given by

$$\mathcal{E}_b = 16\gamma\sqrt{1-\omega^2}. \tag{3.5}$$

In two dimensions the equation is not integrable. In addition there is the complication of the boundaries. Therefore the only relations that can be used are conservation laws, and in particular the conservation of energy. When the kink is in branch 1, its energy is $8w_1\gamma$ because it is homogeneous in the transverse direction. Similarly in branch 2, it has energy $8w_2\gamma_2$. The conservation of energy reads

$$w_1\frac{8}{\sqrt{1-v_1^2}} = 2w_2\frac{8}{\sqrt{1-v_2^2}}, \tag{3.6}$$

where we assumed $w_2 = w_3$. This expression gives a critical velocity v_1 for which $v_2 = 0$:

$$v_k = \sqrt{1-\left(\frac{w_1}{2w_2}\right)^2}. \tag{3.7}$$

This formula was derived in [8] and compared successfully to the 2D numerical results for a fixed angle and widths $w_3 = w_1$, $0 < w_2/w_1 < 1$. In the next section we confirm this estimate by numerical simulations and show its limitations.

A similar argument for the breather yields the following result for the parameters $\{v_1, \omega_1\}$ in the bottom branch and the parameters $\{v_2, \omega_2\}$ in the top branches

$$\frac{v_1^2 - 1}{\omega_1^2 - 1} = \Big(\frac{w_1}{2w_2}\Big)^2 \frac{v_2^2 - 1}{\omega_2^2 - 1}. \tag{3.8}$$

This gives a critical velocity v_1 for which $v_2 = 0$

$$v_k = \sqrt{1 - \frac{\omega_1^2 - 1}{\omega_2^2 - 1}\Big(\frac{w_1}{2w_2}\Big)^2}. \tag{3.9}$$

The practical application of the previous formula is difficult because ω_2 remains unknown. Note however that for small amplitudes, i.e. in the linear limit $\omega_1 = \omega_2$ so that we recover (3.7) for the critical velocity.

4. Numerical methods

We first consider the propagation of a kink in Y- and T-junctions. As expected the kink gets reflected if it does not have enough energy (velocity). Also the motion depends very weakly on the angle. To illustrate this fact, we show in Fig. 4 a kink propagating in a T-junction and crossing it. We take the same kink and run it into a Y-junction. This is shown in Fig. 5. One can see that the time intervals for propagation are about the same. This is confirmed by examining the evolution of the energy in the branches 1 (bottom) and 2 (left), see Fig. 6. Note also that a very small amount of energy, typically 5% of the total energy, is left in branch 1 once the kink has crossed over into branches 2 and 3. The solution of the 1D effective model is plotted with points in Fig. 6; it agrees very well with the 2D solution and this confirms the informal asymptotic reduction from 2D to 1D of the previous section.

We now compare systematically the 2D solution with the one of the 1D effective equation. To validate this approximation, we conduct a parametric study choosing w_1, w_2 and w_3 such that $w_1 = 1$, $w_2 = w_3 = w_1 + \alpha$ where $\alpha = -0.3, -0.1, 0.1, 0.3$. The results for the critical velocity as well as the estimate (3.7) are reported in the Table 1. The 2D and 1D models are very close even for $\alpha > 0$. On the other hand the energy estimate is a lower estimate for $\alpha > 0$, The 2D and 1D effective results reveal that the kink crosses the junction but that there are oscillations. The front seems to oscillate and then reshape as it enters more into branches 2 and 3. We do not see this effect when $\alpha \leq 0$. Despite this, the values are all within a 10% interval of error.

To check the 2D-1D reduction even further, we conducted simulations with a large width $w_1 = w_2 = w_3 = 10$ for large and small velocities. We found that for a small velocity $v_1 = 0.75$ the kink gets reflected and significant transverse oscillations occur. These transverse oscillations are the ones that propagate along the equal phase contour lines; they were studied by Gulevitch *et al.* [9] who showed that their dispersion is $\omega = k$. In this situation, the angle becomes important and of course the 2D and the 1D models

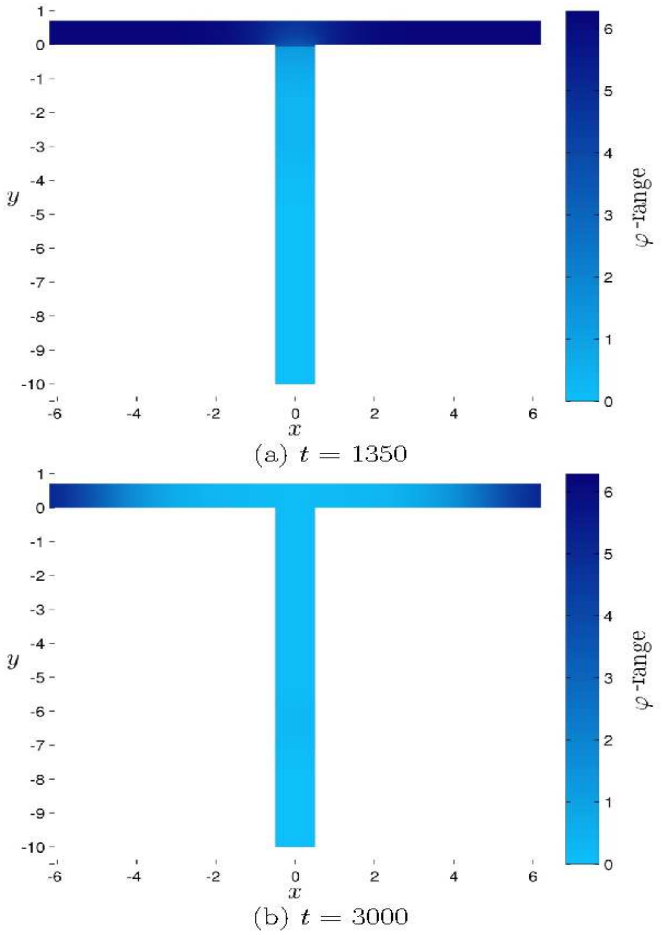

Figure 4. *Motion in a T-junction. Snapshots of a kink starting in branch 1 with a velocity* $v_1 = 0.75$. *The times are* $t = 1350$ *(a) and* $t = 3000$ *(b) .*

α	2D v_c	1D v_c	v_k from (3.7)
0.3	0.98	0.99	0.92
0.1	0.965	0.955	0.89
0	0.92	0.94	0.86
-0.1	0.885	0.85	0.83
-0.3	0.73	0.71	0.7

Table 1. *Kink critical velocities for the 2d model, the 1d effective model and the energy estimate as a function of* α. *The widths of the branches are* $w_1 = 1$, $w_2 = w_3 = w_1 + \alpha$.

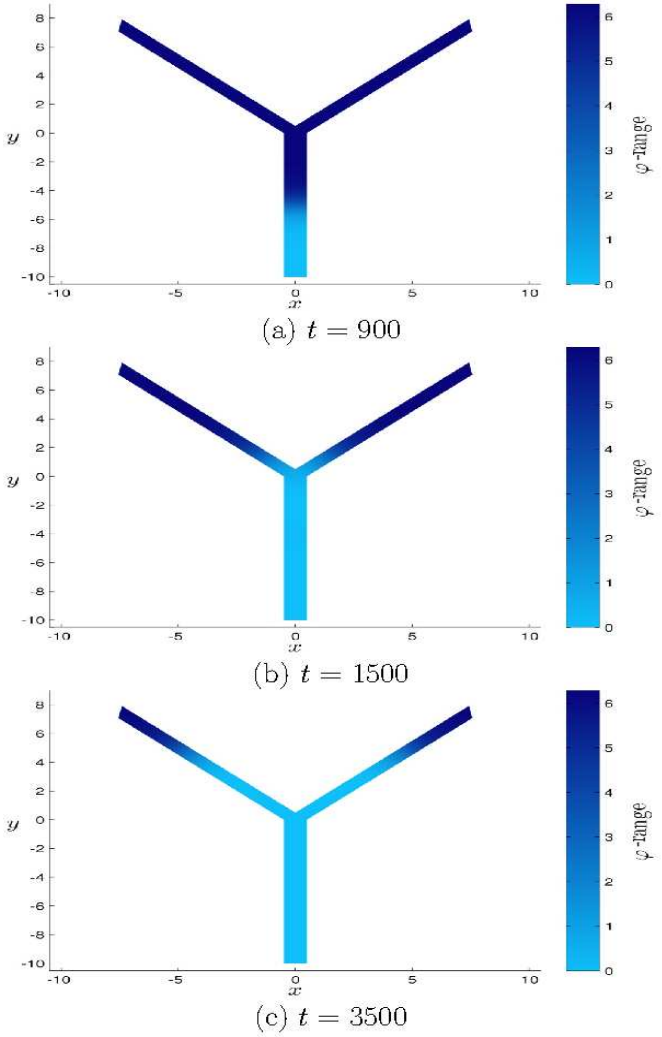

Figure 5. *Motion of a kink in a* 90° *Y-junction. Snapshots of a kink starting in branch 1 with a velocity* $v_1 = 0.75$. *The times are* $t = 900$ *(a),* $t = 1500$ *(b) and* $t = 3500$ *(c). The widths are* $w_1 = 1,\ w_2 = w_3 = 0.7$.

disagree. On the other hand, for a large velocity $v_1 = 0.96$, the kink crosses and the transverse oscillations remain small. Then the 2D and the 1D models are very close.

For the breather, things are more complicated because of the additional parameter, the frequency. The energy criterion is not sufficient, the breather needs to have the adapted frequency in order to cross. To illustrate this, we consider a breather of initial velocity $v_1 = 0.4$ and different frequencies. Fig. 7 shows the energy E_1 in branch 1 as a function of time for frequencies $\omega_1 = 0.5,\ 0.7, 0.725$ and 0.75. The breather does not cross until the frequency reaches 0.75; for this frequency the initial energy is smaller than for $\omega_1 = 0.5$. The initial energy will not determine crossing, the initial frequency will. Another interesting

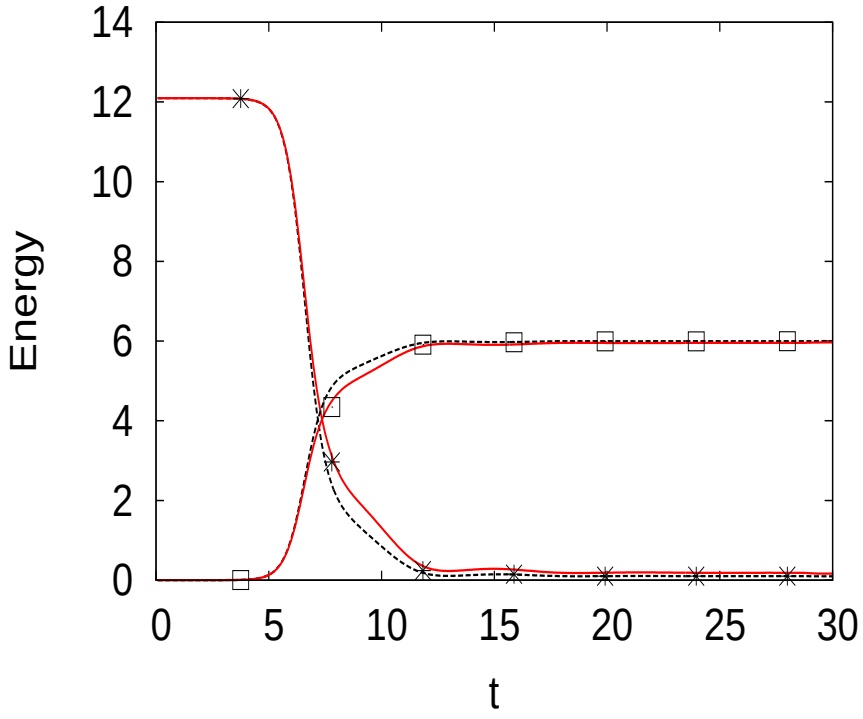

Figure 6. *Time evolution of the energy for the kink motion in branches 1 and 2 for the T-junction in full line (red online) and for the Y-junction in dashed line. The energy for the 1D effective model is plotted with points. The parameters are the same as in Figs. 4 and 5.*

effect is that for $\omega_1 = 0.725$ the energy E_1 almost goes to 0 in the time interval $[200; 300]$ -as if the breather crossed the junction- and then it returns almost to its initial value, indicating reflection. We checked the position of the breather and found that it stays with an interval of size 10 close to the junction. This long oscillation close to the junction could indicate a nonlinear bound state associated to the fork.

Fig. 8 shows the crossing vs. non crossing in the parameter space (v, ω). The crossing (resp. reflection) of the breather is indicated by the + (resp. $\times$) sign. The calculations were done both with the 1D effective model and the full 2D equations and the results always agreed. For large enough velocities, the breather crosses independently of its frequency. On the other hand, for frequencies close to one, the breather crosses even for small velocities. This situation is close to the linear case for which we expect always some energy transfer to the other branch [3].

There is always a small reflection from the fork. For example, we show the time evolution of the energy of a breather in Fig. 9. Notice how the energy in branch 1 does not drop to zero as for the kink. There is a remainder.The small scale oscillations present in Fig. 9 are the ones seen in Fig. 7; at this time we do not know their origin.

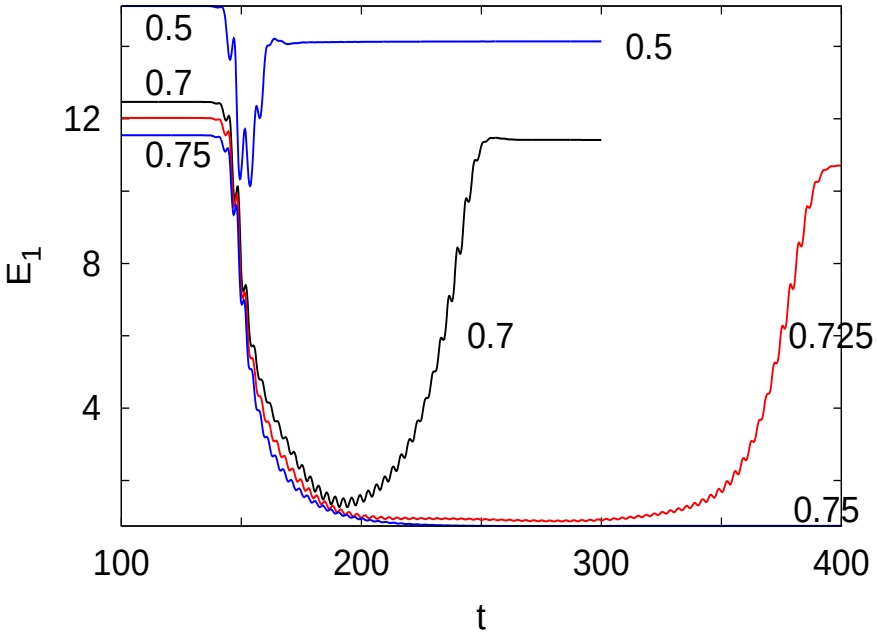

Figure 7. *Energy in branch 1 as a function of time for the 1D model and a breather of initial velocity* $v_1 = 0.4$ *and frequencies* $\omega_1 = 0.5,\ 0.7, 0.725$ *and* 0.75. *Notice the crossing for* $\omega_1 = 0.75$. *The widths are* $w_1 = w_2 = w_3 = 1$.

To characterize the breathers in the other branches is difficult because the wave oscillates. We found that plotting the energy density

$$\mathrm{d}\mathcal{E} = \frac{1}{2}\phi_t^2 + \frac{1}{2}\phi_x^2 + 1 - \cos\phi, \tag{4.1}$$

gives a good indication of the position of the breather. Let us analyze in more details the specific configuration where a breather of speed $v = 0.8$ and frequency $\omega = 0.3$ crosses the junction. Fig. 10 shows the energy density for three different times in the branch 1 (top panel) and in the branch 2 (bottom panel) after the breather has passed the junction. Then the energies in branch 1 and branch 2 are respectively $\mathcal{E}_1 = 2.16$ and $\mathcal{E}_2 = 13.23$. The velocities estimated by a least square fit on the center of mass of the breather density are respectively $v_1 = -0.75$ and $v_2 = 0.6$. They are lower than the initial velocity to accommodate for the crossing of the breather. The frequencies of the breathers in branches 1 and 2 can be estimated, they are respectively $\omega_1 = 0.996$ and $\omega_2 = 0.75$. All these parameters are very different from the initial breather parameter making the scattering of a breather much more complex than the one of a kink.

Using the parameters above we can plot the fitted breathers and compare them with the numerical solution. Fig. 11 shows in the top panel, branch 1 before the breather crosses. There the analytical solution matches perfectly the numerical one. The middle and bottom panels show respectively branch 1 after the crossing and branch 2. Here the agreement is not as good but remains quite acceptable. The reflected breather in branch 1 (middle

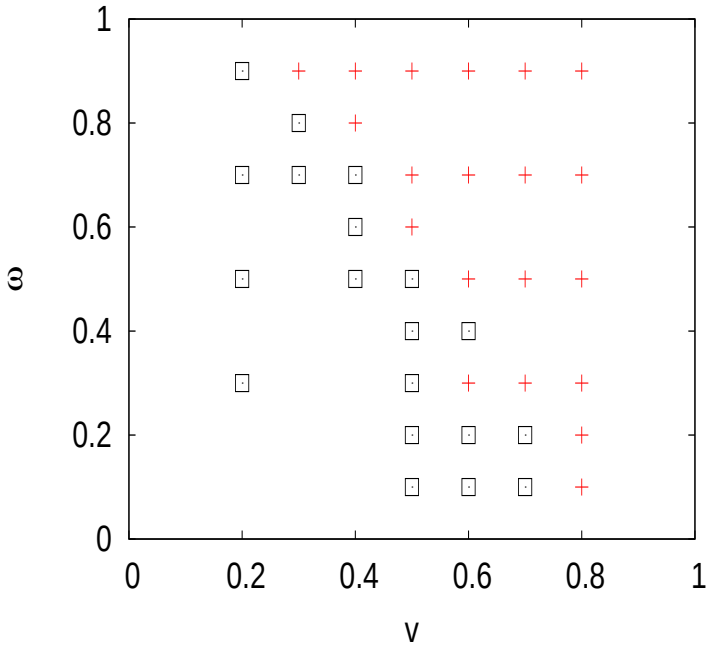

Figure 8. *Parameter space (v, ω) for the crossing of breathers for the 2D and the 1D models. The crosses (red online) indicate crossing and the squares reflection. The widths are $w_1 = w_2 = w_3 = 1$.*

panel) has a small amplitude of about 0.2. Its frequency as seen from Table 2 is 0.99 so that it is very close to the dispersion curve $\omega = \sqrt{1 + k^2}$. This can explain the dispersion observed.

To conclude this study we examine systematically the influence of the breather frequency on its crossing. We took $v_1 = 0.8$ and chose $\omega_1 = 0.3$, 0.5, 0.7 and 0.9. The results are reported in Table 2.

5. Conclusion

We analyzed numerically and theoretically how a 2D sine-Gordon kink or breather crosses a Y- or T–junction. Comparing the energies in the different branches for both cases revealed that the angle of the junction plays almost no role in the dynamics for thin trees. This suggested to introduce a 1D effective model where at the junction, we satisfy continuity of the solution and flux conservation. The solutions of this effective model accurately reproduce the 2D solutions.

The parameters for the kink to cross obey the simple relation obtained from the conservation of energy. There is a critical velocity below which no crossing is possible.

Breather crossing is more complex because there are two parameters: the velocity v and frequency ω. For equal widths of the branches, we observe crossing when $v > 1 - \omega$.

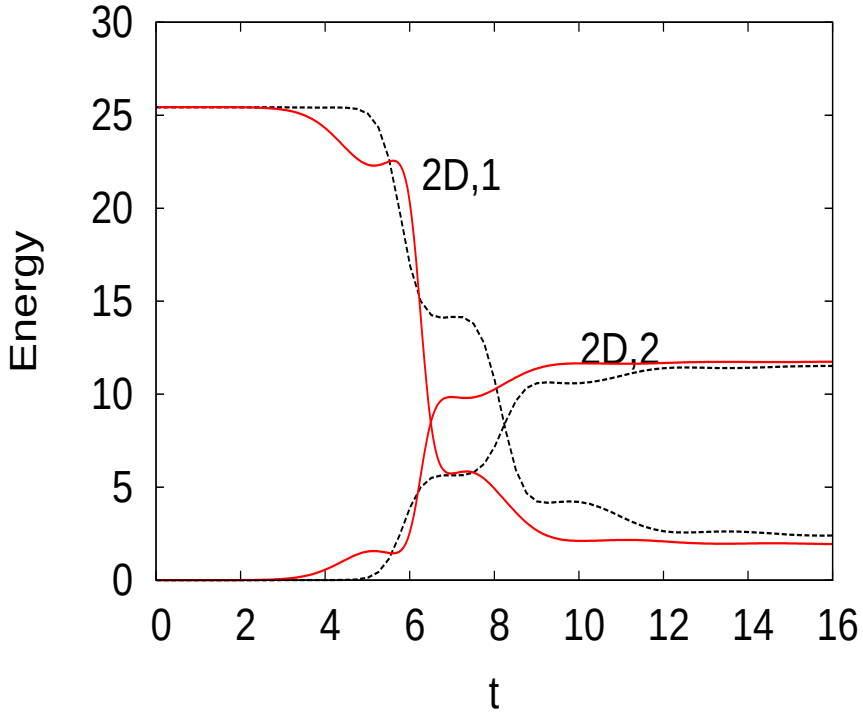

Figure 9. *Time evolution of the energy in branches 1 and 2 for a breather for the 2d partial differential equation in full line (red online) and the 1d effective model in dashed line. The parameters are* $w_1 = w_2 = w_3 = 1$, $v_1 = 0.8, \omega_1 = 0.3, x_0 = 10$.

branch index i	1	1-return	2		1	1-return	2
ω_i	0.3	0.99	0.79		0.5	0.99	0.87
v_i	0.8	0.8	0.56		0.8	0.8	0.65
energy $\mathcal{E}$	25.42	2.1	11.66		23.07	2.12	10.48
ω_i	0.7	0.998	0.93		0.9	0.999	0.98
v_i	0.8	0.85	0.73		0.8	0.85	0.8
energy $\mathcal{E}$	19.03	1.91	8.57		11.61	1.23	5.192

Table 2. *Velocities and frequencies for the crossing of a breather of initial velocity* $v_1 = 0.8$ *and different frequencies* $\omega_1 = 0.3$, 0.5 *(top rows) and* $\omega_1 = 0.7$, 0.9 *(bottom rows). The columns indicate the branches, 1, "1-return" and 2. The label "1-return" corresponds to branch 1 after the collision.*

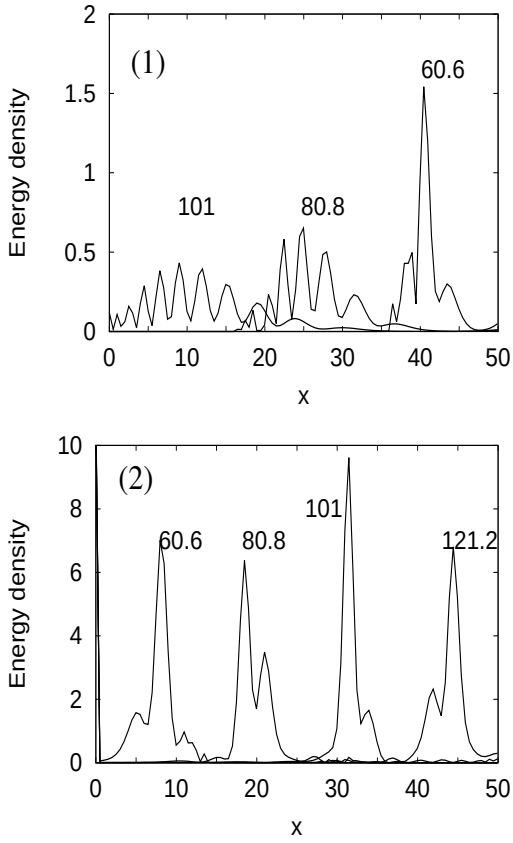

Figure 10. *Snapshots of the energy density of a breather at different times in branches 1 (top) and 2 (bottom). The times are indicated on the plots. The parameters are* $w_1 = w_2 = w_3 = 1, v_1 = 0.8, \omega_1 = 0.3$. *The initial position of the breather is* $x_0 = 10$.

Then the breather gives rise to two other breathers in the two upper branches that we characterize using the energy density and the value of the energy. These new breathers are slower than the initial condition and are also up-shifted in frequency. We always observe a small reflexion at the crossing into the first branch.

This study can be extended by considering more branches. Another interesting extension would be to add a source at the junction, enabling to control the crossing. It would be useful to understand how to transpose this to another application, like the reflexion of shallow water waves.

Acknowledgments

D. Dutykh acknowledges the support from ERC under the research project ERC-2011-AdG 290562-MULTIWAVE and thanks INSA de Rouen for its hospitality during his visit in

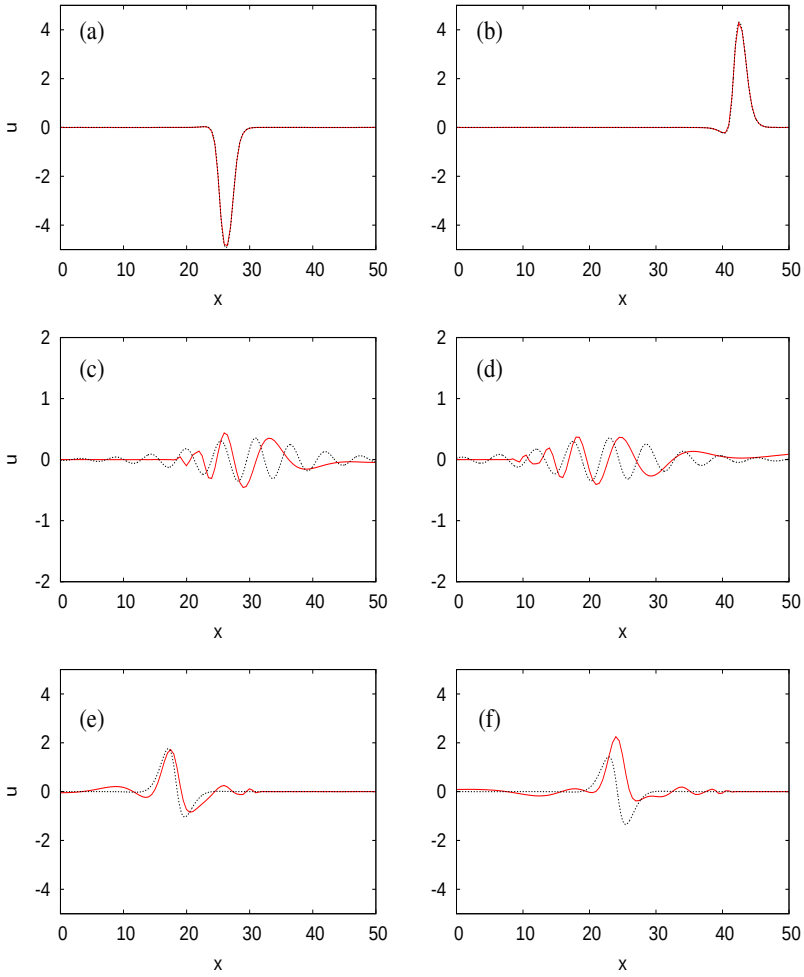

Figure 11. *Snapshots of the breather analytical solution (dashed line)together with the numerical solution (continuous line), in branch 1 before the collision (top panels a,b), in branch 1 after the collision (middle panels c,d) and in branch 2 (bottom panels e,f). The corresponding times are* $t = 20.2,\ 40.4,\ 80.8,\ 90.9$ *for panels (a, b, c, d) and* $t = 80.8,\ 90.9$ *for panels (e,f).*

December 2012. The authors thank D. Mitsotakis and G. Sadaka for useful discussions on the finite element numerical method. The authors acknowledge the Centre de Ressources Informatiques de Haute Normandie where most of the calculations were done.

References

[1] S. Backhaus and M. Chertkov. Getting a grip on the electrical grid. *Physics Today*, 66(5):42, 2013. 5

[2] A. Barone and G. Paternò. *Physics and Applications of the Josephson Effect*. Wiley-VCH Verlag GmbH & Co. KGaA, Weinheim, FRG, July 1982. 5

[3] P. N. Bibikov and L. V. Prokhorov. Mechanics not on a manifold. *J. Phys. A: Math. Gen*, 42(4):045302, Jan. 2009. 5, 13

[4] J. L. Bona and R. Cascaval. Nonlinear dispersive waves on trees. *Canadian Applied Mathematics Quarterly*, 16(1):1–18, 2008. 5

[5] J.-G. Caputo, A. Knippel, and E. Simo. Oscillations of networks: the role of soft nodes. *J. Phys. A: Math. Gen.*, 46(3):035101, Jan. 2013. 6

[6] R. K. Dodd, J. C. Eibeck, J. D. Gibbon, and H. C. Morris. *Solitons and Nonlinear Wave Equations*. Academic Press, 1984. 9

[7] S. Gnutzmann and U. Smilansky. Quantum graphs: Applications to quantum chaos and universal spectral statistics. *Advances in Physics*, 55(5-6):527–625, July 2006. 5

[8] D. Gulevich and F. Kusmartsev. Flux Cloning in Josephson Transmission Lines. *Phys. Rev. Lett.*, 97(1):017004, July 2006. 5, 9

[9] D. Gulevich, F. Kusmartsev, S. Savel'ev, V. Yampol'skii, and F. Nori. Shape Waves in 2D Josephson Junctions: Exact Solutions and Time Dilation. *Phys. Rev. Lett*, 101(12):127002, Sept. 2008. 10

[10] F. Hecht. New development in Freefem++. *Journal of Numerical Mathematics*, 20(3-4):251–266, Jan. 2012. 5

[11] D. Mugnolo and J.-F. Rault. Construction of exact travelling waves for the Benjamin-Bona-Mahony equation on networks. *Submitted*, pages 1–18, 2013. 5

[12] A. Nachbin and V. Da Silva Simoes. Solitary waves in open channels with abrupt turns and branching points. *J. Nonlinear Math. Phys.*, 19:1240011, Jan. 2012. 5

[13] W. Nichols, M. O'Rourke, and C. Vlachopoulos. *McDonald's Blood Flow in Arteries*. CRC Press, London, sixth edition, 2011. 5

[14] A. Scott. *Nonlinear Science: Emergence and Dynamics of Coherent Structures*. Oxford University Press, 2nd edition, 2003. 5, 8

Laboratoire de Mathématiques, INSA de Rouen,, 76801 Saint-Etienne du Rouvray, France
E-mail address: caputo@insa-rouen.fr
URL: https://sites.google.com/site/jeanguycaputo

LAMA, UMR 5127 CNRS, Université de Savoie, Campus Scientifique, 73376 Le Bourget-du-Lac Cedex, France
E-mail address: Denys.Dutykh@univ-savoie.fr
URL: http://www.denys-dutykh.com/